Report

Current Biology

Actin-Based Transport Adapts Polarity Domain Size to Local Cellular Curvature

Graphical Abstract

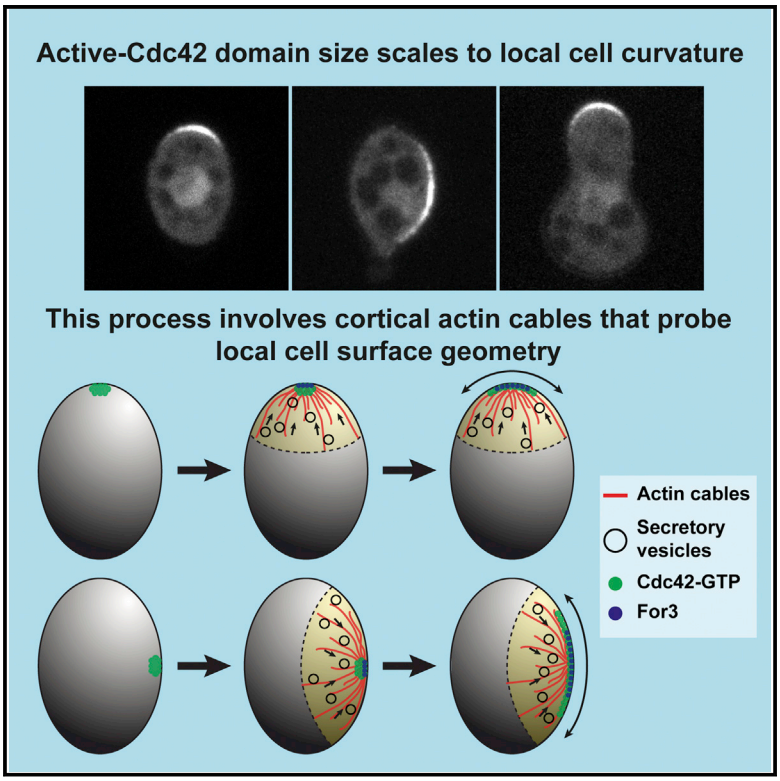

Highlights

- How cells probe their shape and size to scale intracellular structures is not known
- Cortical polarity domains scale their width to local cell-surface curvature
- This geometrical effect depends on vesicle transport along cortical actin cables
- The area scanned by actin cables grown on a curved surface may explain this scaling

Authors

Daria Bonazzi, Armin Haupt, Hirokazu Tanimoto, Delphine Delacour, Delphine Salort, Nicolas Minc

Correspondence

nicolas.minc@ijm.fr

In Brief

Bonazzi et al. show that Cdc42-GTP polarity domains scale their size to local cell-surface radii of curvature. This effect depends on cortical actin cables that transport secretory vesicles to these domains. These data suggest that actin networks can probe cell curvature to adapt the size of functional polar domains to cell sizes and shapes.

Bonazzi et al., 2015, Current Biology *25*, 1–7
October 19, 2015
http://dx.doi.org/10.1016/j.cub.2015.08.046

CellPress

Please cite this article in press as: Bonazzi et al., Actin-Based Transport Adapts Polarity Domain Size to Local Cellular Curvature, Current Biology (2015), http://dx.doi.org/10.1016/j.cub.2015.08.046

Current Biology
Report

Actin-Based Transport Adapts Polarity Domain Size to Local Cellular Curvature

Daria Bonazzi,[1,3] Armin Haupt,[1,3] Hirokazu Tanimoto,[1] Delphine Delacour,[1] Delphine Salort,[1,2] and Nicolas Minc[1,*]
[1]Institut Jacques Monod, 15 Rue Hélène Brion, 75205 Paris Cedex 13, France
[2]Université Pierre et Marie Curie, 15 Rue de l'Ecole de Médecine, 75205 Paris Cedex 06, France
[3]Co-first author
*Correspondence: nicolas.minc@ijm.fr
http://dx.doi.org/10.1016/j.cub.2015.08.046

SUMMARY

Intracellular structures and organelles such as the nucleus, the centrosome, or the mitotic spindle typically scale their size to cell size [1]. Similarly, cortical polarity domains built around the active form of conserved Rho-GTPases, such as Cdc42p, exhibit widths that may range over two orders of magnitudes in cells with different sizes and shapes [2–6]. The establishment of such domains typically involves positive feedback loops based on reaction-diffusion and/or actin-mediated vesicle transport [3, 7, 8]. How these elements may adapt polarity domain size to cellular geometry is not known. Here, by tracking the width of successive oscillating Cdc42-GTP domains in fission yeast spores [9], we find that domain width scales with local cell-surface radii of curvature over an 8-fold range, independently of absolute cell volume, surface, or Cdc42-GTP concentration. This local scaling requires formin-nucleated cortical actin cables and the fusion of secretory vesicles transported along these cables with the membrane. These data suggest that reaction-diffusion may set a minimal domain size and that secretory vesicle transport along actin cables may dilute and extend polarity domains to adapt their size to local cell-surface curvature. This work reveals that actin networks may act as micrometric curvature sensors and uncovers a generic morphogenetic principle for how polarity domains define their size according to cell morphologies.

RESULTS AND DISCUSSION

Cdc42-GTP Polarity Domains Scale Their Width to Local Cell-Surface Curvature

To understand how cells may control the size of a polarity domain, we exploited the oscillatory dynamics of active Cdc42-GTP polar domains/caps in the early development of fission yeast spores, which occurs within an extended G1 phase [9] (Movie S1). We took images of fields of spores expressing CRIB-3GFP, a marker for Cdc42-GTP [10], and developed a semi-automatic script to selectively analyze spores with single domains and compute the full width at half maximum of the domain (FWHM) from a Gaussian fit of the CRIB-3GFP intensity profile along the cell surface [11–13] (Figures 1A and S1A–S1E).

In wild-type (WT) spores, which come with natural variations in shapes and sizes, we found an interesting positive correlation between domain width and cellular local radius of curvature (R_C) measured around the domain (R^2 = 0.59; Figures S1F and S1G). This correlation was well represented by a linear scaling such that FWHM = 0.97 μm + 1.30 × R_C (n = 110 domains; fitting accuracy: R^2 = 0.35; Figure 1B). Cdc42 visualized with a functional sandwich GFP fusion, as well as the Cdc42 GEF Scd1p, the scaffold protein Scd2p, and other upstream polarity components formed domains that followed similar size scaling, with slightly different slopes between markers [9, 14, 15] (Figures S1H and S1I). Importantly, given that the oscillatory dynamics of these domains is much faster than shape changes in those spores, these scaling relationships predominantly reflect an adaptation of domain size to cell geometry, rather than a change in local shape consequent to persistent growth around the site of Cdc42-GTP accumulation [4, 16] (Figure S1J; Movie S1). 3D reconstructions revealed that domains had circular shapes in most instances, although we did observe a fraction of ellipsoidal domains in spores with flattened 3D shapes. The major axes of these ellipsoidal domains appeared to scale with corresponding principal radii of curvature in 3D (Figure S2A). Analysis of spores of the Rho GAP mutants *rga4Δ* and *rga2Δ*, which are respectively bigger and smaller than WT spores [9], allowed to extend the range of validity of this scaling and suggested that domain width scaling was independent of fine-tuned Cdc42 activity (Figure 1B) [4, 10, 17].

To directly manipulate local curvature independently of cell size, we first deformed spores in microfabricated wells or linear microchannels [18–20]. Domains became small when assembling at the curved tip and large when forming on the flat side of deformed spores (Figures 1C and S2B). These experiments showed that domain size was only weakly correlated with cell volume (R^2 = 0.22), surface area (R^2 = 0.23), and uncorrelated with absolute CRIB-3GFP intensity at the cap (R^2 = −0.03; Figure S2C). Second, we analyzed domain size in early repolarizing WT spheroplasts [16, 21]. Those spheroplasts come with similar volumes as vegetative cells but significantly larger radii of curvature at the site of Cdc42-GTP domain assembly. Domains were much larger than those found at cell tips of control cells and also scaled with R_C, suggesting this effect is not a particular property of spores (Figure 1D).

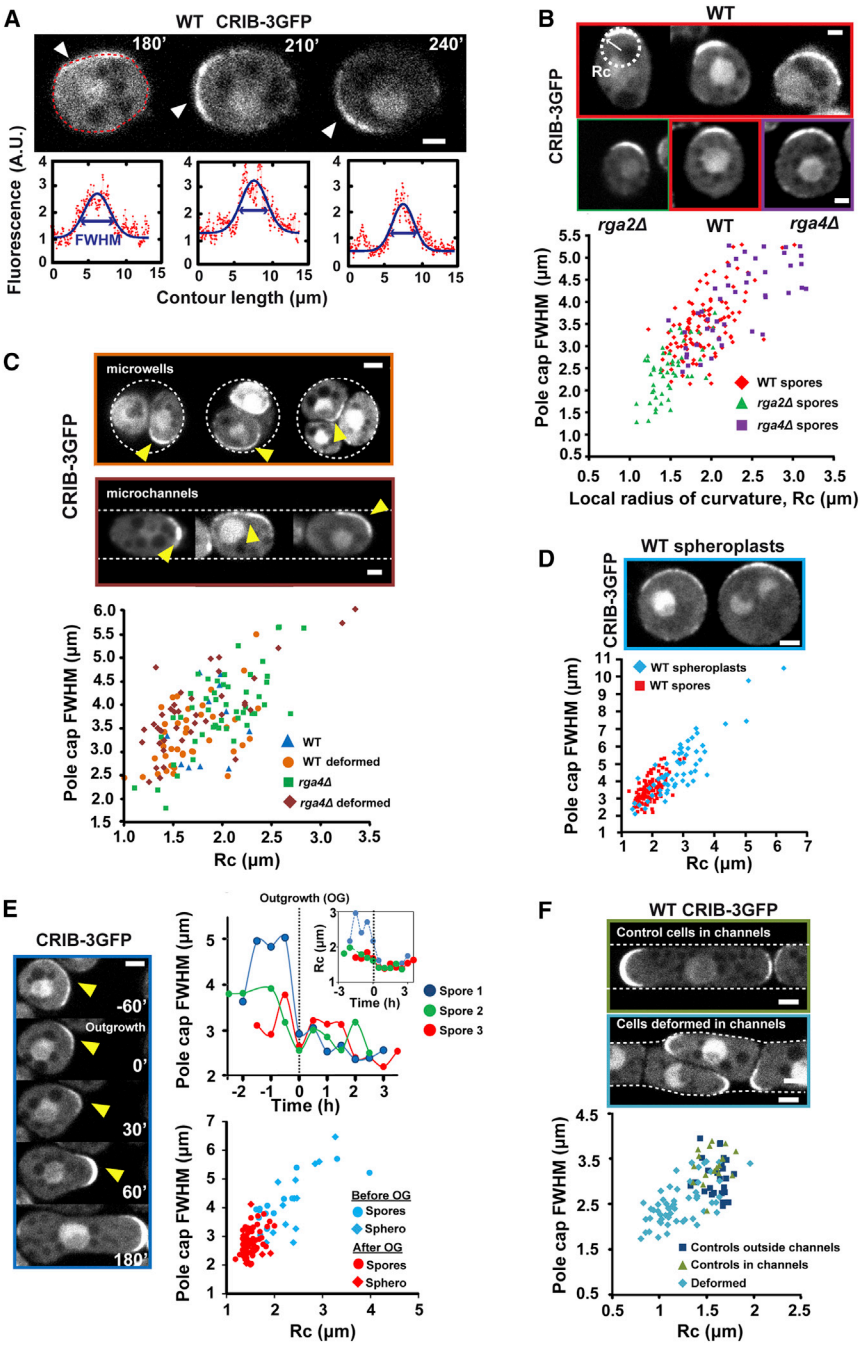

Figure 1. Cdc42-GTP Polar Domains/Caps Scale Their Widths to Local Cellular Radius of Curvature

(A) (Top) Confocal time-lapse of a germinating WT spore expressing CRIB-3GFP. The red dotted line indicates the line scan used to compute fluorescence intensity. (Bottom) Intensity profiles (red dots) and Gaussian fits (blue line) for each time frame of the above time-lapse are shown. The blue double-headed arrow indicates the full width at half maximum (FWHM) of the Gaussian fit.

(B) (Top) Confocal single slice images of WT (red), *rga2Δ* (green), and *rga4Δ* (purple) spores. The white arrow and circle represent the fitting used to compute local radius of curvature (R_C). (Bottom) CRIB-3GFP domain FWHM plotted as a function of R_C for *rga2Δ* (n = 52), WT (n = 110), and *rga4Δ* (n = 45) is shown.

(C) (Top) Confocal single-slice images of spores deformed in microfabricated wells (WT, orange) and microchannels (*rga4Δ*, red). (Bottom) CRIB-3GFP domain FWHM plotted as a function of R_C for WT controls (n = 11) and deformed (n = 41) and *rga4Δ* controls (n = 50) and deformed (n = 40) is shown.

(D) (Top) Confocal images of repolarizing WT spheroplasts. (Bottom) CRIB-3GFP domain FWHM plotted as a function of R_C for WT spheroplasts (n = 60) and spores (n = 110) is shown.

(E) (Left) Confocal time-lapse of outgrowing WT spores expressing CRIB-3GFP. (Right top) Evolution of CRIB-3GFP FWHM as a function of time for three outgrowing spores is shown. (Inset) Evolution of R_C as a function of time for the same spores is shown. (Right bottom) CRIB-3GFP domain FWHM plotted as a function of R_C for different time points before and after outgrowth for WT spheroplasts (n = 2 cells) and spores (n = 8 cells) is shown.

(F) (Top) Confocal single-slice images of undeformed (green) and deformed (light blue) WT cells grown in microchannels. (Bottom) Plot of CRIB-3GFP domain FWHM as a function of R_C for WT cells outside channels (n = 26), undeformed inside channels (n = 18), and deformed inside channels (n = 56) is shown.

The scale bars represent 2 μm.

We then tested whether this scaling remained valid during polarized growth, such as after spore or spheroplast outgrowth, when polarity becomes stable to promote tube extension [9, 16]. Using time-lapses, we found that domain size scaled with R_C at each time point from typically 2 or 3 hr before until 2 or 3 hr after outgrowth. The robustness of the scaling was particularly striking close to outgrowth, when the pointy tip emerged out of the spore or spheroplast body, as R_C rapidly transited from large to small values to eventually plateau at a value half of the typical WT diameter [9, 16] (Figure 1E). These results suggest that the diameter of emerging polar tubes is not firmly pre-set by the size of Cdc42-GTP domains before tube emergence but rather relies on more dynamic crosstalk between geometry and domain size or other unknown elements (Figure S2D) [4, 16]. Accordingly, by manipulating the diameter of polarized vegetative WT cells in microchannels, we could generate cells with diameters much smaller than controls, which exhibited smaller Cdc42-GTP domains well scaled to curvature radii at the tips (Figure 1F). We conclude that domain size adaptation to local curvature also applies to stable polar growth situations.

Pulling together those different conditions, we validated domain sizing over almost an 8-fold range (from R_C = 0.80 μm to R_C = 6.23 μm), with an overall scaling law following FWHM = 0.81 μm + 1.42 × R_C (n = 557 domains; fitting accuracy: R^2 = 0.68; Figure S2E). Thus, Cdc42-GTP domains can probe local

surface geometry to adapt their width to micrometric cellular curvatures.

Secretory Vesicle Transport along Actin Cables Adapts Domain Size to Local Curvature

Cytoskeleton polymers may contribute to the assembly and maintenance of polarity domains [14]. Although microtubule depolymerization did not impact domain size and scaling, we found that complete actin disassembly with 100 μM Latrunculin A (LatA) had a major impact on domain size. Cdc42-GTP domains still oscillated [9] and were polarized in similar fraction as in controls but were significantly smaller. Importantly, these LatA-treated domains did not adapt their widths to curvature but remained small independently of cell geometry (R^2 = 0.01; Figures 2A–2C, 3C, and S3A). Dynamic LatA wash-in caused domains to shrink to a minimal size independent of their initial width. Conversely, LatA wash-outs yielded domain expansion, and width recovery adapted to local curvature (Figures 2D and 2E).

In yeast, actin contributes to Cdc42 polarity by regulating Cdc42 endocytosis at Arp2/3-nucleated actin patches and secretory vesicle transport along formin-nucleated cables that carry Cdc42 and/or other factors toward the membrane [14]. In *for3Δ* spores, which lack For3-nucleated actin cables, Cdc42-GTP domain size was smaller than WT and did not scale with local curvature ($R^2 = -0.01$). A *sec8-1* mutant, which strongly reduces secretory vesicle fusion at restrictive temperature [22, 23], displayed a similar phenotype as *for3Δ*, with even smaller domains (Figures 3A–3C and S3A–S3C). In contrast, endocytosis did not impact domain scaling, as tested with various endocytic mutants or with short-time treatment with 100 μM of CK666, which disrupts actin patches (Figures 3C and S3D) [24]. Altogether, these results suggest that an actin-independent system may assemble polarity domains with a minimal size and that secretory vesicles transport along actin cables and their fusion at the membrane may extend these domains to scale them to local curvature.

Vesicle Transport and Fusion May Dilute Cdc42-GTP Domains in a Curvature-Dependent Manner

How vesicle transport and fusion may contribute to Cdc42 polarization is still debated. One model posits that vesicles may deliver more Cdc42 to the domain [3], whereas another one suggests that vesicle fusion may instead dilute polar domains [25]. Recent work has challenged the delivery model by showing that a Cdc42 allele, $Cdc42^{SW}$-rit^{C}, that is not trafficked on secretory vesicles is still capable of spontaneous Cdc42-GTP polarization [15]. In this allele, we found that domains still adapted their width to local curvature, with a scaling close to the WT situation. LatA treatment caused similar shrinkage and loss of scaling as in WT (Figures 3D, 3E, S3E, and S3F). Thus, the traffic of Cdc42 itself on secretory vesicles is dispensable for domain size adaptation to local curvature.

To test whether vesicle transport and fusion may rather dilute polarity domains, we compared Cdc42-GTP concentration in subsequent domains, formed at different locations in the same spore using time-lapses. We found that a transition from a first, narrow domain assembled on a curved region to a second, wide domain formed on a flatter region was accompanied by a significant decrease in CRIB signal. Conversely, a transition from a wide to a narrow domain yielded an increase in CRIB signal (Figures 3F and 3G). These findings are consistent with a mechanism in which vesicle transport and fusion may dilute and extend Cdc42-GTP domains in a curvature-dependent manner.

A Model Based on the Limitation of Vesicle Transport by the Surface Scanned by Actin Cables May Explain Domain Size Adaptation to Local Curvature

We next visualized actin cables associated with Cdc42-GTP domains [26]. Actin cables had wiggly appearance with varying lengths and were quite dynamic, with a typical turn-over of tens of seconds (Figure S4A). Notably, 3D analysis revealed that the vast majority of cables were restricted to a cortical region within 0.4 μm underneath the plasma membrane, in agreement with a previous report in budding yeast (Figures 4A–4C and S4B; Movie S2) [27]. This cortical actin cable arrangement may thus represent an optimal configuration to probe cell-surface geometry.

Actin cable nucleation by the formin For3p did not appear to be sensitive to curvature. For3-3GFP exhibited a dotty pattern clustered in a single domain, which scaled with R_C (Figure 4D). To estimate cable number and length distributions, we treated cells with CK666, which does not influence domain sizing at short timescales (Figure 3C), to selectively disassemble patches that obscure the visualization of cables and then imaged after 5 min [24]. In agreement with for3-3GFP results, the number of actin cables connected to the polarity domain increased on average with R_C (Figure 4E). Actin cable lengths, computed in 3D, followed similar distributions independently of local curvature (Figure 4F). Together, these results suggest that, in varying spore surface geometries, actin cable networks may grow with similar nucleation density, stability, and length distribution.

Given that cortical actin cables turn over within seconds and that polarity domains establish within minutes, the network of cables associated with Cdc42-GTP caps may scan on average a dome-like surface, which depends on cable length distribution and local surface geometry. Simple mathematical analysis suggested that the surface covered by these ''domes'' displayed a steady increase with R_C in the range of curvature radii and cable length measured in spores (Figures 4C, 4G, 4H, and S4B; supplemental model). Given this, we propose a simple geometrical model for cap size adaptation to local geometry based on four components (Figure 4H). (1) Actin cables dynamically radiate from sites of Cdc42-GTP accumulation along the cell surface and have a length distribution independent of curvature (observation; mechanism unknown). (2) Vesicles flux toward the cap increases with the area scanned by actin domes (hypothesis). (3) Cdc42-GTP caps are built by an actin-independent system and diluted by secretory vesicles (observation). (4) Dilution extends the cap in proportion to vesicle flux (hypothesis; supported by previous theoretical work) [28].

In sum, our quantitative analyses of oscillating Cdc42-GTP caps in fission yeast spores serve to define mechanisms for how cortical domains may set their size with respect to cellular geometry. Domains can still assemble without actin, most likely through reaction-diffusion, and have a minimal size independent of curvature [29]. In these spores, actin is thus dispensable for spontaneous Cdc42 polarization [8, 15] but may function

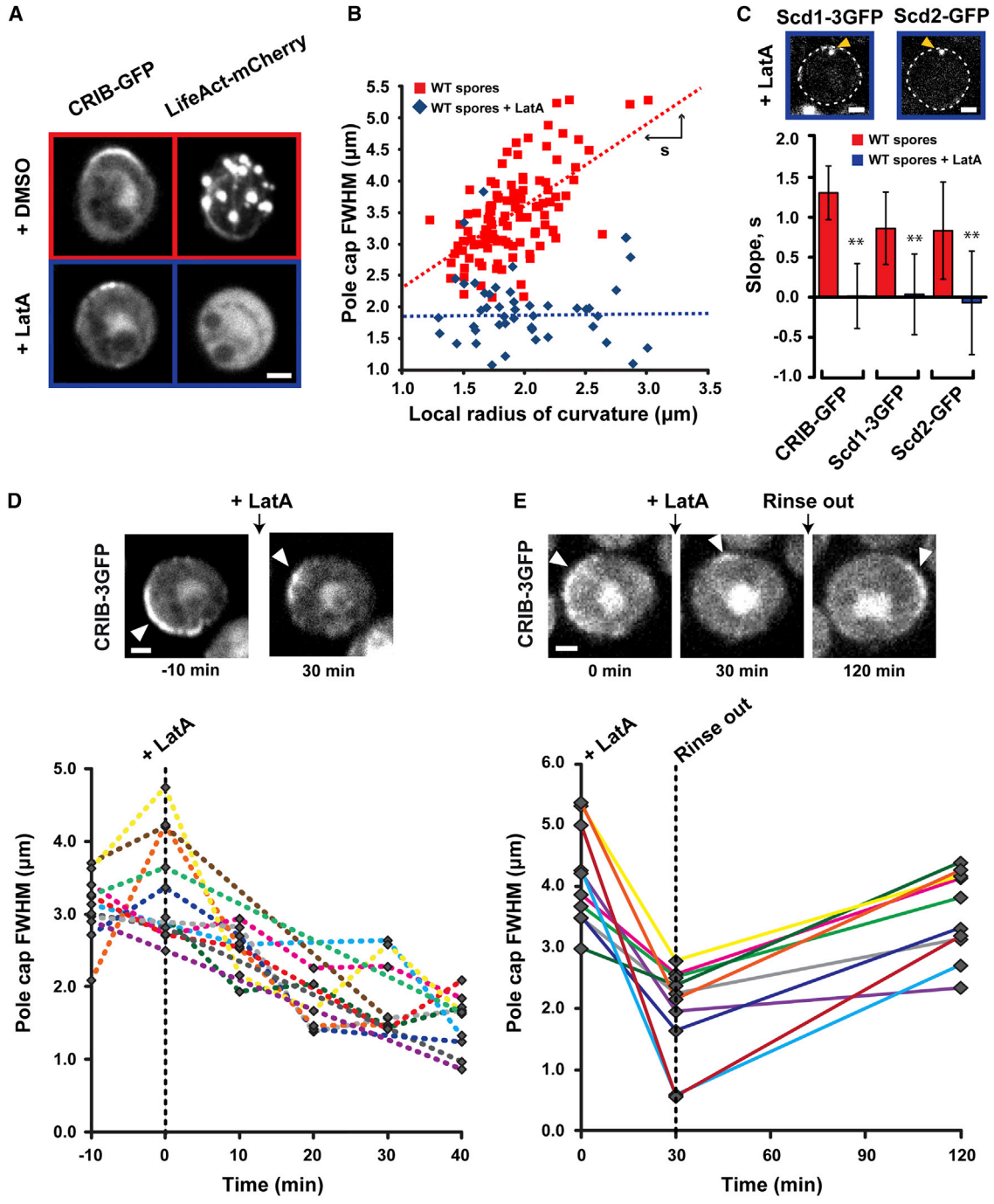

Figure 2. Actin Mediates Polar Domain Size Scaling to Cellular Curvature

(A) WT spores expressing CRIB-3GFP (confocal single slices) and LifeAct-mCherry (merged stacks) treated with DMSO (red) or 100 μM Latrunculin A (LatA) (blue).

(B) Plot of CRIB-3GFP FWHM as a function of R_C for controls (n = 110) and spores treated with LatA for 30 min in bulk (n = 52). Dotted lines represent corresponding linear fits with slopes (s).

(C) (Top) Confocal single-slice images of LatA-treated WT spores expressing Scd1-3GFP or Scd2-GFP. Arrowheads mark polar domains. (Bottom) Linear regression slopes for CRIB-3GFP, Scd1-3GFP, and Scd2-GFP in controls (n = 110 for CRIB-3GFP; n = 39 for Scd1-3GFP; n = 14 for Scd2-GFP) and LatA-treated spores (n = 52 for CRIB-GFP; n = 30 for Scd1-3GFP; n = 30 for Scd2-GFP). Error bars represent SD of regression values. **Student's t test $p < 10^{-5}$.

(D) (Top) Confocal time-lapse of a spore expressing CRIB-3GFP 10 min before and 30 min after LatA treatment. (Bottom) Evolution of CRIB-3GFP domain FWHM as a function of time following LatA wash-in for 12 individual WT spores is shown.

(E) (Top) Confocal time-lapse of a spore expressing CRIB-3GFP before LatA treatment, 30 min after LatA wash-in, and 90 min after wash-out. (Bottom) Evolution of CRIB-3GFP domain FWHM as a function of time following LatA treatment and wash-out for ten individual wild-type spores is shown.

The scale bars represent 1 μm.

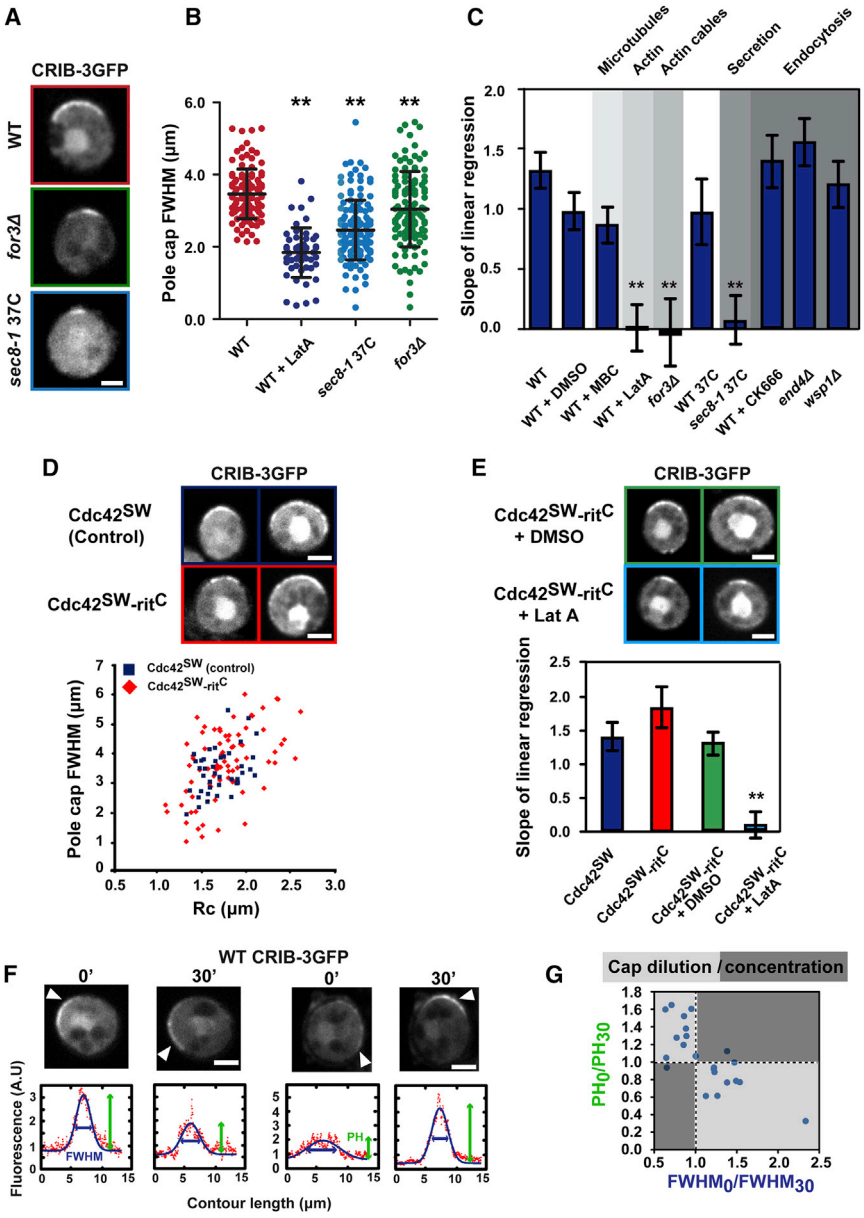

Figure 3. Actin-Cables-Based Secretory Vesicle Transport and Fusion May Dilute Polarity Domains to Scale Them to Local Curvature

(A) Confocal single-slice images of WT, *for3Δ*, and *sec8-1* (37°C) spores expressing CRIB-3GFP.

(B) Polarity domain sizes for control WT (n = 110), WT treated with LatA (n = 52), *sec8-1* (n = 131), and *for3Δ* spores (n = 108).

(C) Linear regression slopes of CRIB-3GFP domain size scaling as a function of R_C in the indicated mutants and drug treatments (n > 30 for each condition). Error bars represent SD.

(D) (Top) Confocal mid-plane images of CRIB-3GFP-expressing spores carrying the Cdc42-mCherry^{SW} (blue) or Cdc42-mCherry^{SW}-rit^{C} (red) allele. (Bottom) Plot of CRIB-3GFP domain FWHM as a function of R_C for Cdc42-mCherry^{SW} (n = 42) and Cdc42^{SW}-rit^{C} (n = 77) spores is shown.

(E) (Top) Confocal images of Cdc42-mCherry^{SW}-rit^{C} spores expressing CRIB-3GFP treated with DMSO (green) or LatA (light blue). (Bottom) Linear regression slopes for Cdc42-mCherry^{SW} (n = 42), Cdc42-mCherry^{SW}-rit^{C} (n = 77), Cdc42-mCherry^{SW}-rit^{C} + DMSO (n = 22), and Cdc42^{SW}-rit^{C} + LatA (n = 43) spores are shown.

(F) (Top) Confocal single-slice time-lapse of two individual WT spores expressing CRIB-3GFP, taken at 0 and 30 min, normalized in the same manner. (Bottom) Corresponding intensity profiles (red dots) and Gaussian fits (blue line) for each time frame of the above time-lapse are shown. The blue and green double-headed arrows indicate FWHM and peak height (PH) of the Gaussian fit, respectively.

(G) Ratio of peak height between 0 min and 30 min (PH_0/PH_{30}) plotted against ratio of FWHM ratio ($FWHM_0/FWHM_{30}$) for n = 22 individual spores. Quadrants of the plot correspond to dilution of CRIB signal in the cap (light gray) or concentration of CRIB signal in the cap (dark gray).

**Student's t test $p < 10^{-5}$. The scale bars represent 2 μm.

primarily to adapt domain size to local cell geometry. We propose that actin cable network growth on differently curved surfaces may yield sufficient variations in the surface scanned by the network to influence the flux of secretory vesicles back to the domain and consequent domain sizing. Thus, in our view, curvature sensing is not encoded at the level of cytoskeleton polymer structural properties [30] but rather as a result of self-organization of the network on a given surface geometry [31].

Whereas recent studies have suggested that the fission yeast diameter is set by the size of Cdc42-GTP domains [4, 16], our data refine these views and demonstrate that domains can also rapidly adapt to cell morphology, highlighting novel functional interplays between shape and polarity [18, 20]. Accordingly, recent theoretical models predict the existence of stability conditions on the adaptation of Cdc42-GTP domain size to cell geometry required to maintain a stable diameter over generations of dividing cells [12]. Finally, by analyzing images of active-Cdc42 domains in other cell types, we found that our scaling could be valid over a 100-fold range in radii of curvature (Figures S4C and S4D) [2–6]. Because most eukaryotic cells share the use of Rho GTPases and actin-based systems to cluster functional cortical domains, our study may have uncovered a novel generic design for morphogenesis.

SUPPLEMENTAL INFORMATION

Supplemental Information includes Supplemental Experimental Procedures, one supplemental model, four figures, and two movies and can be found with this article online at http://dx.doi.org/10.1016/j.cub.2015.08.046.

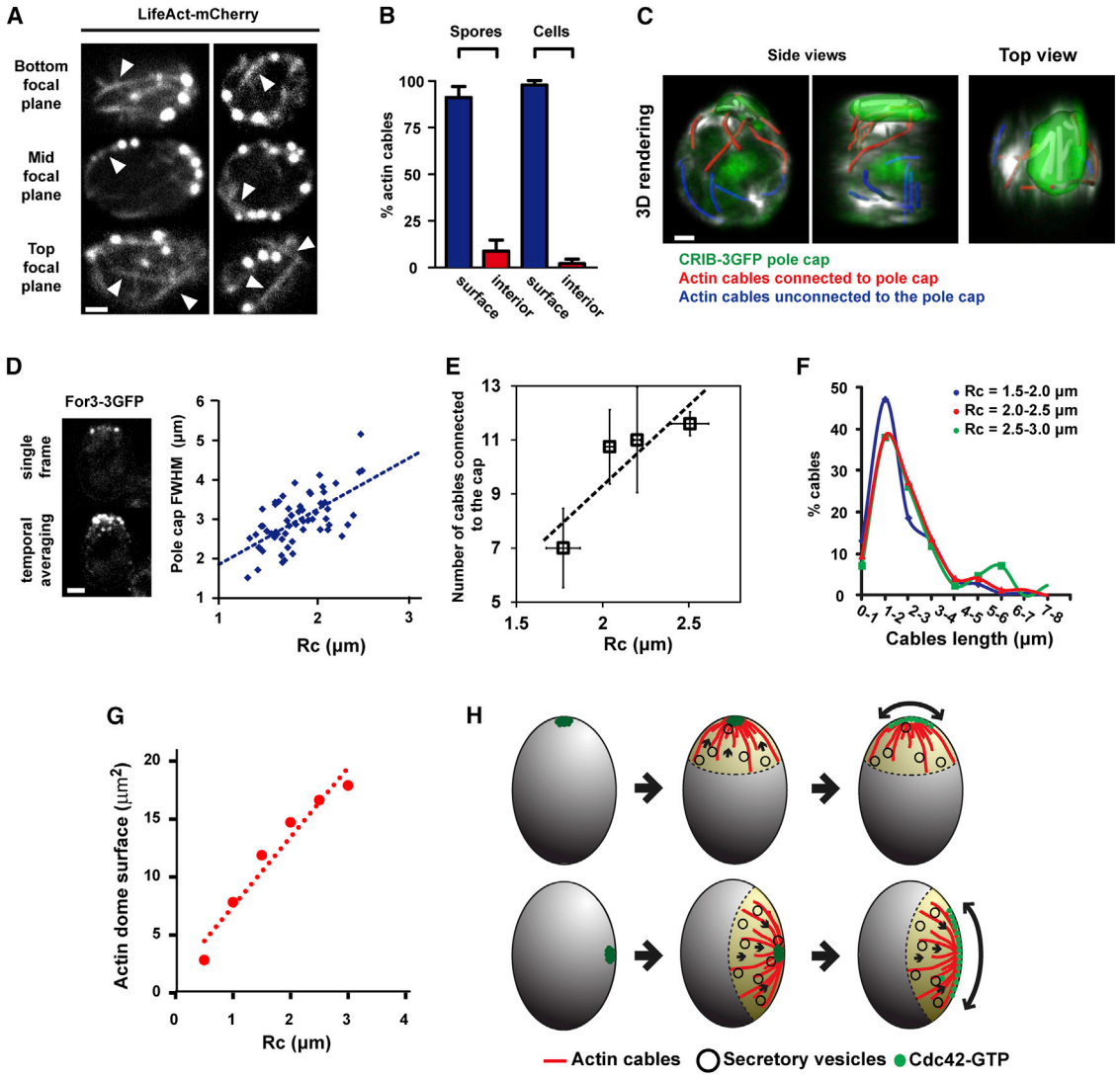

Figure 4. Cortical Actin Cable Networks May Probe Local Cell-Surface Geometry to Scale Polarity Domains to Local Radii of Curvature

(A) Confocal slices of spores expressing LifeAct-mCherry at the bottom, mid, and top focal plane. White arrowheads point at actin cables.

(B) Actin cables localization for spores and cells (n > 10 in each condition).

(C) 3D rendering of a WT spore expressing LifeAct-mCherry and CRIB-3GFP 5 min after CK666 treatment.

(D) (Top left) Single mid-focal confocal image of a WT spore expressing For3-3GFP. (Bottom left) Corresponding temporally averaged picture obtained by a projection of 30 single images taken every 1 s is shown. (Right) For3-3GFP domain FWHM plotted as a function of R_C quantified from temporally averaged For3-3GFP domains (n = 62) is shown.

(E) Number of actin cables connected to Cdc42-GTP caps as a function of R_C in WT spores (n = 10 spores and 141 cables).

(F) Distribution of actin cable length connected to Cdc42-GTP domains binned with respect to R_C (n = 21 spores and 296 cables).

(G) Evolution of actin dome's surface as a function of R_C mathematically computed and weighted to account for cables length distribution measured in (F).

(H) Deformation of actin networks growing on a surface with a given geometry may account for polarity domain size adaptation to local curvature: an initial Cdc42-GTP domain with minimal size is assembled by reaction-diffusion; actin cables then grow from this domain following the curvature of the local surface and define over time a dome-like network from where they fetch vesicles that move back to the domain along cables. Fusion of these vesicles expands the Cdc42-GTP domain via a dilution mechanism. The surface explored by these actin cables over time may influence the flux of vesicles carried back to the domain. As a consequence, an actin network grown on a flat surface may bring more vesicles to the domain than on a curved surface, yielding a broader polarity domain. Error bars represent SD.

The scale bars represent 1 μm.

AUTHOR CONTRIBUTIONS

D.B., A.H., D.D., and N.M. performed experiments; H.T. developed image analysis scripts; and D.B., A.H., D.S., and N.M. designed the experiments. D.B., A.H., H.T., and N.M. wrote the manuscript.

ACKNOWLEDGMENTS

The authors acknowledge S. Martin, M. Balasubramanian, and F. Martin-Belmonte for sharing material. We thank G. Romet-Lemonne and A. Jegou for careful reading of the manuscript. We acknowledge the ImagoSeine facility,

a member of France BioImaging (ANR-10-INSB-04), and V. Contremoulins for help with Imaris. Our laboratory is supported by the CNRS and grants from the FP7 CIG program, ITN "FungiBrain," the "Mairie de Paris emergence" program, FRM "amorçage" (AJE20130426890), and the European Research Council (CoG Forcaster no. 647073).

Received: March 17, 2015
Revised: July 31, 2015
Accepted: August 20, 2015
Published: October 1, 2015

REFERENCES

1. Levy, D.L., and Heald, R. (2012). Mechanisms of intracellular scaling. Annu. Rev. Cell Dev. Biol. *28*, 113–135.
2. Dehapiot, B., Carrière, V., Carroll, J., and Halet, G. (2013). Polarized Cdc42 activation promotes polar body protrusion and asymmetric division in mouse oocytes. Dev. Biol. *377*, 202–212.
3. Wedlich-Soldner, R., Altschuler, S., Wu, L., and Li, R. (2003). Spontaneous cell polarization through actomyosin-based delivery of the Cdc42 GTPase. Science *299*, 1231–1235.
4. Kelly, F.D., and Nurse, P. (2011). Spatial control of Cdc42 activation determines cell width in fission yeast. Mol. Biol. Cell *22*, 3801–3811.
5. Neukomm, L.J., Zeng, S., Frei, A.P., Huegli, P.A., and Hengartner, M.O. (2014). Small GTPase CDC-42 promotes apoptotic cell corpse clearance in response to PAT-2 and CED-1 in C. elegans. Cell Death Differ. *21*, 845–853.
6. Lichius, A., Goryachev, A.B., Fricker, M.D., Obara, B., Castro-Longoria, E., and Read, N.D. (2014). CDC-42 and RAC-1 regulate opposite chemotropisms in Neurospora crassa. J. Cell Sci. *127*, 1953–1965.
7. Mogilner, A., Allard, J., and Wollman, R. (2012). Cell polarity: quantitative modeling as a tool in cell biology. Science *336*, 175–179.
8. Irazoqui, J.E., Gladfelter, A.S., and Lew, D.J. (2003). Scaffold-mediated symmetry breaking by Cdc42p. Nat. Cell Biol. *5*, 1062–1070.
9. Bonazzi, D., Julien, J.D., Romao, M., Seddiki, R., Piel, M., Boudaoud, A., and Minc, N. (2014). Symmetry breaking in spore germination relies on an interplay between polar cap stability and spore wall mechanics. Dev. Cell *28*, 534–546.
10. Tatebe, H., Nakano, K., Maximo, R., and Shiozaki, K. (2008). Pom1 DYRK regulates localization of the Rga4 GAP to ensure bipolar activation of Cdc42 in fission yeast. Curr. Biol. *18*, 322–330.
11. Das, M., Drake, T., Wiley, D.J., Buchwald, P., Vavylonis, D., and Verde, F. (2012). Oscillatory dynamics of Cdc42 GTPase in the control of polarized growth. Science *337*, 239–243.
12. Drake, T., and Vavylonis, D. (2013). Model of fission yeast cell shape driven by membrane-bound growth factors and the cytoskeleton. PLoS Comput. Biol. *9*, e1003287.
13. Klünder, B., Freisinger, T., Wedlich-Söldner, R., and Frey, E. (2013). GDI-mediated cell polarization in yeast provides precise spatial and temporal control of Cdc42 signaling. PLoS Comput. Biol. *9*, e1003396.
14. Martin, S.G., and Arkowitz, R.A. (2014). Cell polarization in budding and fission yeasts. FEMS Microbiol. Rev. *38*, 228–253.
15. Bendezú, F.O., Vincenzetti, V., Vavylonis, D., Wyss, R., Vogel, H., and Martin, S.G. (2015). Spontaneous Cdc42 polarization independent of GDI-mediated extraction and actin-based trafficking. PLoS Biol. *13*, e1002097.
16. Kelly, F.D., and Nurse, P. (2011). De novo growth zone formation from fission yeast spheroplasts. PLoS ONE *6*, e27977.
17. Villar-Tajadura, M.A., Coll, P.M., Madrid, M., Cansado, J., Santos, B., and Pérez, P. (2008). Rga2 is a Rho2 GAP that regulates morphogenesis and cell integrity in S. pombe. Mol. Microbiol. *70*, 867–881.
18. Terenna, C.R., Makushok, T., Velve-Casquillas, G., Baigl, D., Chen, Y., Bornens, M., Paoletti, A., Piel, M., and Tran, P.T. (2008). Physical mechanisms redirecting cell polarity and cell shape in fission yeast. Curr. Biol. *18*, 1748–1753.
19. Zegman, Y., Bonazzi, D., and Minc, N. (2015). Measurement and manipulation of cell size parameters in fission yeast. In Biophysical Methods in Cell Biology, E. Paluch, ed. (Academic Press).
20. Minc, N., Bratman, S.V., Basu, R., and Chang, F. (2009). Establishing new sites of polarization by microtubules. Curr. Biol. *19*, 83–94.
21. Flor-Parra, I., Zhurinsky, J., Bernal, M., Gallardo, P., and Daga, R.R. (2014). A Lallzyme MMX-based rapid method for fission yeast protoplast preparation. Yeast *31*, 61–66.
22. Wang, H., Tang, X., Liu, J., Trautmann, S., Balasundaram, D., McCollum, D., and Balasubramanian, M.K. (2002). The multiprotein exocyst complex is essential for cell separation in Schizosaccharomyces pombe. Mol. Biol. Cell *13*, 515–529.
23. Bendezú, F.O., and Martin, S.G. (2011). Actin cables and the exocyst form two independent morphogenesis pathways in the fission yeast. Mol. Biol. Cell *22*, 44–53.
24. Burke, T.A., Christensen, J.R., Barone, E., Suarez, C., Sirotkin, V., and Kovar, D.R. (2014). Homeostatic actin cytoskeleton networks are regulated by assembly factor competition for monomers. Curr. Biol. *24*, 579–585.
25. Layton, A.T., Savage, N.S., Howell, A.S., Carroll, S.Y., Drubin, D.G., and Lew, D.J. (2011). Modeling vesicle traffic reveals unexpected consequences for Cdc42p-mediated polarity establishment. Curr. Biol. *21*, 184–194.
26. Huang, J., Huang, Y., Yu, H., Subramanian, D., Padmanabhan, A., Thadani, R., Tao, Y., Tang, X., Wedlich-Soldner, R., and Balasubramanian, M.K. (2012). Nonmedially assembled F-actin cables incorporate into the actomyosin ring in fission yeast. J. Cell Biol. *199*, 831–847.
27. Yu, J.H., Crevenna, A.H., Bettenbühl, M., Freisinger, T., and Wedlich-Söldner, R. (2011). Cortical actin dynamics driven by formins and myosin V. J. Cell Sci. *124*, 1533–1541.
28. Savage, N.S., Layton, A.T., and Lew, D.J. (2012). Mechanistic mathematical model of polarity in yeast. Mol. Biol. Cell *23*, 1998–2013.
29. Orlandini, E., Merenduzzo, D., and Goryachev, A.B. (2013). Domain formation on curved membranes: phase separation or Turing patterns? Soft Matter *9*, 9311–9318.
30. Ursell, T.S., Nguyen, J., Monds, R.D., Colavin, A., Billings, G., Ouzounov, N., Gitai, Z., Shaevitz, J.W., and Huang, K.C. (2014). Rod-like bacterial shape is maintained by feedback between cell curvature and cytoskeletal localization. Proc. Natl. Acad. Sci. USA *111*, E1025–E1034.
31. Théry, M., Pépin, A., Dressaire, E., Chen, Y., and Bornens, M. (2006). Cell distribution of stress fibres in response to the geometry of the adhesive environment. Cell Motil. Cytoskeleton *63*, 341–355.